The nature of the chalcogen colour centres in ultramarine-type solids

Dirk Reinen and Gottlieb-Georg Lindner

Fachbereich Chemie und Zentrum für Materialwissenschaften, Philipps-Universität, D-35043 Marburg

Received (in Cambridge) 20th July 1998

Blue minerals and gems have always been subjects of fascination to man. In particular lapislazuli is and was highly esteemed and also used as a precious stone and as a pigment. The host compound is the zeolite-type sodalite and the colour centres are S_2^- and S_3^-, whose amount ratio determines the specific hue, varying from violet blue to blue to green. But Se_2^- can also be substituted into the sodalite cages in high percentages, giving the pigment a brilliant red colour. It is even possible to incorporate the rather voluminous radical species Te_2 and Te_2^- into the sodalite matrix. Because the otherwise unstable colour centres are completely screened from the atmosphere and isolated from each other in the cages, they can be fully characterised by various spectroscopic techniques.

1 Introduction

Blue-hued minerals[1] have long played an important role in the cultural history of mankind and have perpetually fascinated man. The oldest precious stone of this kind is 'Lapislazuli', which was already in use in the Sumerian civilisation about 5500 years ago, the name being a strange mixture of the Latin word for stone (lapis) and the Persian notation for blue (lazur). The underlying pigment is 'Ultramarine' with the colour centres S_3^- and S_2^- incorporated into the cages of the zeolitic host solid sodalite.[2] The colour purity and the colourfastness explain the high appreciation of lapislazuli, which was valued as gold in ancient Egypt and used as a brilliant though expensive painting colour in the middle ages. It was also widely applied in the European cultures and mainly mined in Afghanistan, a country 'beyond the (Mediterranean) sea'—which may be taken as the synonym of 'Ultramarine'. It took until 1806 for the first reliable analysis to be accomplished, suggesting that sulfur species were the colour centres. The earliest syntheses of blue ultramarines were performed in 1826 by J. B. Guimet and C. G. Gmelin,[3] and in 1834 C. Leverkus founded the first plant manufacturing ultramarine in Germany.

A further ancient coloured mineral is 'Egyptian Blue', $CaCuSi_4O_{10}$, one of the first artificial pigments in man's history, and in use in Egypt since 2500 BC. Due to the square-planar $Cu^{II}O_4$ unit as the colour centre[4]—with only parity-forbidden d–d transitions in the visible spectral region—the colour is rather pale and nicely visible in the Queens' crown of Nofretete as the most prominent example with most probably this pigment[5] (Fig. 1). A further common blue pigment in Egypt was 'Azurite' $Cu_3[(CO_3)(OH)]_2$. It was also appreciated as a rather cheap painters' pigment in the middle ages, but has the disadvantage of decomposing to 'Malachite', $Cu_2[(CO_3)(OH)_2]$, by release of CO_2—thus producing unwelcome tinges of green, particularly in blue skies. In the Maya culture in Mexico and Guatemala 'Maya Blue' was in use presumably more than two thousand years ago, as a mural paint and a pottery pigment. It was synthesized by the reaction of the mineral palygorskit and indigo vat, the colour centres being indigo molecules inserted into the open channels of the silicate layer.[6]

With the rapid development of chemistry and the beginning of industrialisation further blue pigments appeared on the

Dirk Reinen is Professor of inorganic solid state chemistry at the Philipps University of Marburg. He graduated in 1960 in Bonn with a thesis on ligand field spectroscopy of transition metal oxide ceramics (supervisor: O. Schmitz-DuMont) and spent two postdoctoral years at North-Western University (Evanston, USA) with P. W. Selwood, working on solid state catalysis. His research interests are manifold, reaching from the electronic structure of 3d metal ions mainly in oxides via *the structural and spectroscopic implications of vibronic interactions (Jahn–Teller effect) to subjects such as superconductivity and colour and constitution of inorganic pigments. He maintains links with institutions throughout the world, particularly in the eastern countries, and was Visiting Professor at some of these places.*

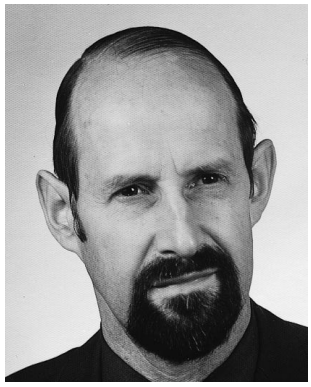

Dirk Reinen

Gottlieb-Georg Lindner received his doctors' degree in 1994 in Marburg with D. Reinen and a thesis title related to that of this article. After one year in Berlin-Adlershof with investigations centred on non-linear optical properties of zeolite-type solids, he spent two years as a Humboldt fellow in the National Institute for Research of Inorganic Materials in Tsukuba, Japan, where he performed syntheses of allophanes and related novel meso-porous materials. Since 1998 he has held a position in industry (DEGUSSA).

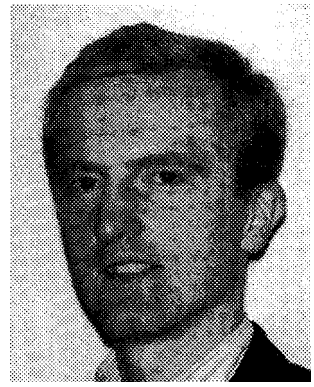

Gottlieb-Georg Lindner

Fig. 1 The Queens' crown of Akhenaten's spouse Nofretete (1360 BC). Reproduced with permission from a slide supplied by the copyright holder Ägyptisches Museum der Staatlichen Museen Berlin Stiftung Preußischer Kulturbesitz.

market—such as 'Prussian Blue', $Fe^{III}_4[Fe^{II}(CN)_6]_3 \cdot nH_2O$ (1704),[7] where the colour originates from intervalence bands between Fe^{II} and Fe^{III}, or 'Cobalt Blue', $CoAl_2O_4$, a spinel in which the tetrahedrally coordinated Co^{II} ions are the colour centres. The latter pigment was first synthesized in Egypt, before it was rediscovered, about 3000 years later, by Thenard (1804). Also to the group of technical pigments belongs 'Manganese Blue' (1903), the colouring agent being MnO_4 tetrahedra isomorphously substituted into the carrier solid $BaSO_4$. It was only recently established that Mn in the oxidation state (+V) is the colour centre.[8] Finally an important recently developed industrial pigment, 'Vanadium Blue' (1948), should be mentioned,[9] whose colour is due to vanadium(IV) on the tetrahedral Si^{IV} position of zirconium silicate $ZrSiO_4$, as has been unequivocally substantiated by EPR and optical spectroscopy[10]—though it has been claimed that the Zr^{IV} position[11a] or interstitial sites[11b] might also be occupied.

2 Blue ultramarines and related compounds

The basic host solid of the ultramarines is the mineral sodalite $Na_8[Al_6Si_6O_{24}]Cl_2$. The blue colour is generated if the radical anions S_2^- and S_3^- substitute partly or completely for the chloride ions,[2] a typical composition being $Na_{6.9(1)}[Al_{5.6(1)}Si_{6.4(1)}O_{24}]S_{2.0(1)}$.[12] The stoichiometry of this ultramarine indicates that nearly exclusively the latter colour centre ($\approx (S_3^-)_{2/3}$) is present. The visible spectrum (Fig. 2,II) is dominated by an absorption band at 16800 cm^{-1} (595 nm), which is correspondingly ascribed to S_3^-. Light absorption occurs in the region above 21500 cm^{-1}, lending a violet-tinged blue colour to the solid. A fine artists' example of this hue is the Russian lapislazuli carving in Fig. 3. A steel-blue colour appears (Fig. 2,I) if the intensity of the weak absorption in the violet spectral region at 26000 cm^{-1}, which originates from the S_2^- radical anion, increases. A wonderful piece of art with this particular hue is the Chinese junk in Fig. 4. In synthetic ultramarines it is possible to further increase the S_2^-/S_3^- ratio by systematic variation of the preparation conditions, generating greenish-blue, turquoise and finally even green colours (Fig. 2,III).[12] Besides the two mentioned centres S_2^- and S_3^-, further

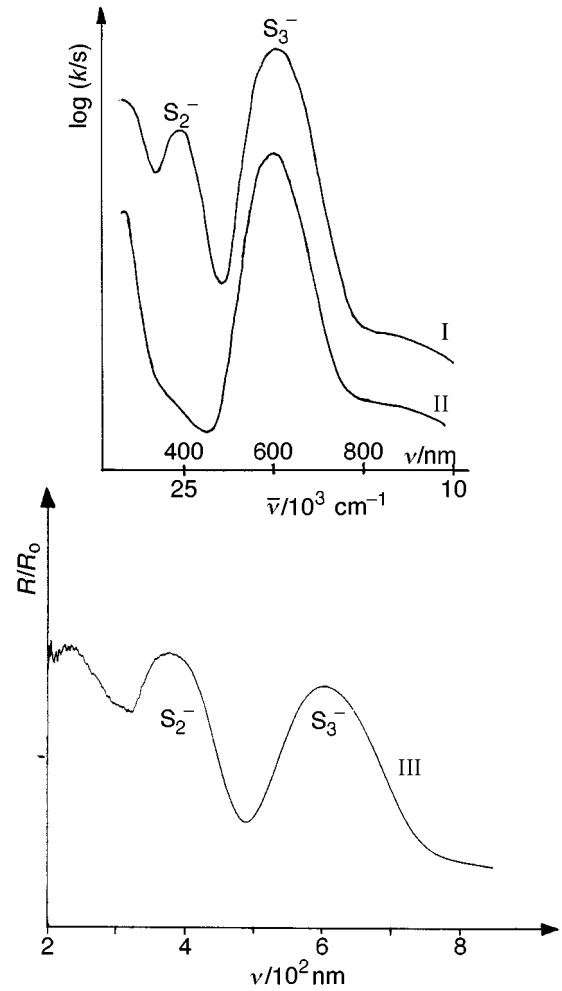

Fig. 2 Powder reflection spectra (298 K) of ultramarines with increasing S_2^-/S_3^- ratio from I to III: violet–blue (II, see Fig. 3), steel-blue (I, see Fig. 4), green (III). The absorption above 30000 cm^{-1} is due to the sodalite framework; the intensity scale is arbitrary - log *k*/s (after Kubelka–Munk) and relative reflectance.

Fig. 3 Decorated Russian lapislazuli carving. Reproduced from reference 14. Copyright 1990, American Museum of Natural History, New York.

radicals are identified by EPR and optical spectroscopy (absorption band at ≈ 19000 cm^{-1}) in synthetic ultramarine-type solids, which are proposed by F. Seel[2] and others[14] to be S_4 and/or S_4^-.

The identification of S_2^- and S_3^- as the main colour species in sulfur ultramarines is the subject of a rather long and controversial history. These radical anions are present as impurity centres in sulfur-doped alkali halide crystals and had already been characterised by their EPR, absorption, IR and resonance Raman spectra 30 years ago.[15,16] The cited basic

Fig. 4 Lapislazuli Chinese junk. Reproduced from reference 14. Copyright 1990, American Museum of Natural History, New York.

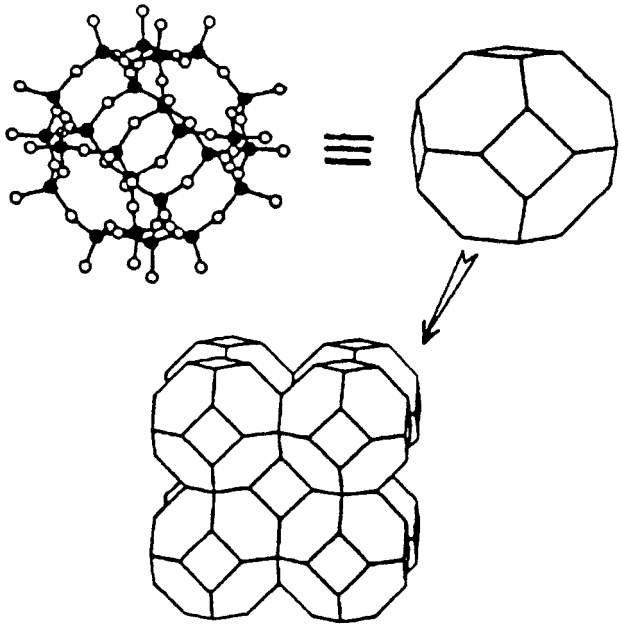

Fig. 5 The cubic cage structure of sodalite $Na_8[Al_6Si_6O_{24}]Cl_2$; $[ClNa_4]^{3+}$ tetrahedra occupy the cage centres.

investigations and many others in the following two decades have essentially facilitated the interpretation of the spectroscopic properties of ultramarine-type solids and the assignment to—which is by now well established—the same S_2^- and S_3^- colour centres.[14]

Fig. 5 depicts the cage structure of the basic sodalite compound. Each cage with the formula $Al_3Si_3O_{12}^{3-}$ is centred by a regular cationic $[ClNa_4]^{3+}$ tetrahedron. If in particular S_3^- substitutes the chloride ions a deficiency is observed on the Cl^- and on the Na^+ positions as well (see the constitution of the above mentioned ultramarine, in which only ≈ 35% of the Cl^- sites are occupied by S_3^-). It can be ascribed to the spacious radical anion causing steric constraints within the cages of limited volume (see below). The sulfur radicals have to be generated simultaneously with the formation of the zeolitic cages in the synthesis procedure, because the latter are impermeable for the colour centres. This property readily explains the extraordinary stability of lapislazuli in spite of the highly unstable di- and trisulfur radical anions. In the related

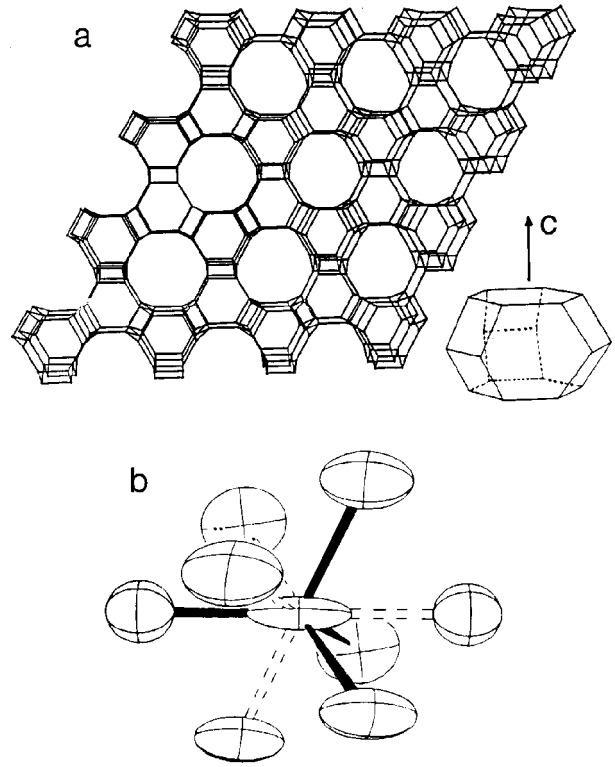

Fig. 6 The hexagonal structure of cancrinite $Na_6Ca[Al_6Si_6O_{24}]CO_3{\cdot}2H_2O$: a single ε-cage and the interconnection pattern, visualising the channels parallel to the crystallographic *c* direction (a); the orientation of the $S_2O_3^{2-}$ anions with respect to *c* in the thiosulfate cancrinite (b).

cancrinite structure (Fig. 6a), which is also composed of cages, they can be created subsequently, however.[17] In contrast to sodalite, the cages form rather open channels parallel to the hexagonal *c*-axis and are porous even for larger species in this direction. The counterions Na^+, Ca^{2+} and CO_3^{2-} as well as the H_2O molecules in this compound are located in the ε-cages shown in Fig. 6a. If carbonate is substituted by thiosulfate, the latter anions orient themselves with their C_3 axes parallel to the channel direction, but disordered in the way shown in Fig. 6b.[17] On irradiation with X-rays the solid turns yellow due to the appearance of an absorption band at 26000 cm^{-1} (see Fig. 2), which indicates the presence of S_2^- radicals. A possible formation mechanism based on a disordered pair of $S_2O_3^{2-}$ anions in neighbouring ε-cages is proposed in eqn. (1). It is

$$[O_3S\text{–}S]^{2-} + [S(\text{–}SO_3]^{2-} \longrightarrow [O_3\dot{S}]^- + [\dot{S}_2]^- + [SO_3]^{2-} \quad (1)$$

further supported by EPR spectroscopy, which clearly shows signals to be assigned to SO_3^- as an additional radical species. Heating the thiosulfate cancrinite at 800 °C in air produces colour changes to green and green–blue caused by the generation of S_3^- as the colour centre besides S_2^-.

Quantum chemical calculations on the free S_2^- and S_3^- radical anions—employing sophisticated techniques for incorporating electron correlation effects—allowed the assignment of the absorption spectra of ultramarine-type solids.[18,19] Fig. 7 gives the one-electron MO scheme for S_2^- and Table 1 comprises the calculated vertical transition energies from the many-electron $^2\Pi_g$ ground state of S_2^- to the low-lying excited doublet terms—only dipole-allowed g ⇔ u transitions are taken into account, together with the corresponding relative dipole transition moments.[18] The main configurational one-electron component of the ground state is the one depicted in Fig. 7, while $^2\Pi_u$ originates essentially from exciting an electron from $\pi_u \rightarrow \pi_g$. The other low-lying excited states included in that study, *i.e.* $^2\Delta_u$, $^2\Sigma_u^-$, $^2\Sigma_u^+$, $^4\Sigma_u^-$, roughly correspond to the excitation of an electron from the π_g into the σ_u MO. It should be noted though, that the simple MO based picture provides

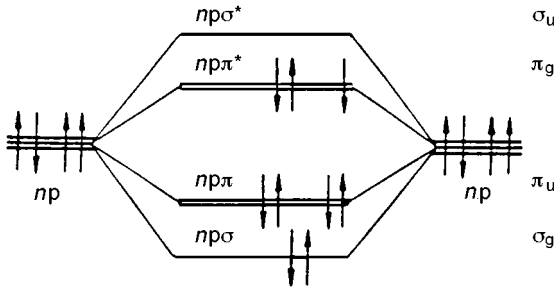

Fig. 7 The molecular orbital scheme of dichalcogen radical anions X_2^- - only MO's resulting from the *n*p–*n*p overlap (*n* = 3, 4, 5 for S, Se, Te) are shown. Electron occupation corresponds to the main MO component of the $^2\Pi_g$ ground state; $\pi_u^4\pi_g^2$ is the main component of the $^3\Sigma_g^-$ ground state of the neutral molecules.

Table 1 Calculated Franck–Condon transition energies[a] for the S_2^- [18] and Se_2^- radical anions,[25] together with the computed relative dipole-transition moments (∥ and ⊥, parallel and perpendicular to the molecular $D_{\infty h}$ axis)

	S_2^-		Se_2^-	
Transition	Franck–Condon transition energies/ 10^3 cm^{-1}	Relative dipole-transition moments	Franck-Condon transition energies/ 10^3 cm^{-1}	Relative dipole-transition moments
$^2\Pi_g{}^b \rightarrow {}^2\Pi_u{}^c$	25.2	1.0 (∥)	18.6	1.0 (∥)
$^2\Pi_g{}^b \rightarrow {}^2\Sigma_u^-{}^d$	24.8	0.4_5 (⊥)	19.7	0.3_5
$^2\Pi_g{}^b \rightarrow {}^2\Delta_u{}^d$	26.0	0.2 (⊥)	20.9	0.2
$^2\Pi_g{}^b \rightarrow {}^2\Sigma_u^+{}^d$	29.3	0.1_5 (⊥)	24.4	0.1

[a] As is common among spectroscopists, wavenumbers are used throughout this contribution as being synonymous with energies, according to the proportionality in the relation: $E = hc\bar{\nu}$. [b, c, d] Main one-electron components (see Fig. 7): $\pi_u^4\pi_g^3\sigma_u^0$, $\pi_u^3\pi_g^4\sigma_u^0$ and $\pi_u^4\pi_g^2\sigma_u^1$, respectively.

only a coarse description for some of these states. The lowest-energy spin-forbidden doublet-to-quartet transition is $^2\Pi_g \rightarrow {}^4\Sigma_u^-$, which is calculated to have an energy below those listed in Table 1 (see Fig. 8). The next doublet terms, connected with the $^2\Pi_g$ ground state by symmetry allowed transitions, are $^2\Pi_u$ (II) and $^2\Sigma_u^-$(II)—mainly originating from exciting one electron from the σ_g into the σ_u MO, and from the two-electron jump $\pi_u^4\pi_g^3\sigma_u^0 \rightarrow \pi_u^2\pi_g^4\sigma_u^1$, respectively (Fig. 7). They are calculated at about 60000 and 77000 cm^{-1}, but are strongly repulsive—no minima in the corresponding potential curves appear (Fig. 8)—and do not need to be considered.[18]

The agreement of the calculated $^2\Pi_g \rightarrow {}^2\Pi_u$ transition energy with the position of the broad band observed at 26000 cm^{-1} (Fig. 2) is rather good, considering that matrix effects are not included in the calculations. Presumably the two lower-intensity transitions $^2\Pi_g \rightarrow {}^2\Sigma_u^-$, $^2\Delta_u$ also contribute to the band intensity (Table 1). As was mentioned before,[15,16] it is also possible to dope S_2^- isomorphously in very small concentrations into the halogenide positions of alkaline chlorides, bromides and iodides, giving rise to a band at a similar energy as that observed in the ultramarines. The $^2\Pi_g \Leftrightarrow {}^2\Pi_u$ transition can be observed in luminescence in the case of sulfur-doped ultramarine type solids as well, inducing a broad emission band around 16000 cm^{-1} (see Fig. 11). The energy difference with respect to the same transition in absorption—the Stokes' shift—is considerable, being about 10000 cm^{-1}, and indicates a large displacement of the respective potential energy curves with respect to each other (Fig. 8). The superimposed progression of ≅ 600 cm^{-1} corresponds to the stretching vibration of the S_2^- colour centre in the $^2\Pi_g$ ground state and is calculated to occur at 582 cm^{-1}.[18]

Similarly well understood are the low-lying electronic states of the S_3^- radical anion. Only the transition $^2B_1 \rightarrow {}^2A_2$ (C_{2v} symmetry) is predicted to occur with sufficiently high intensity at ≅ 17000 cm^{-1},[19] in excellent agreement with the observed band position at the same energy (Fig. 2).

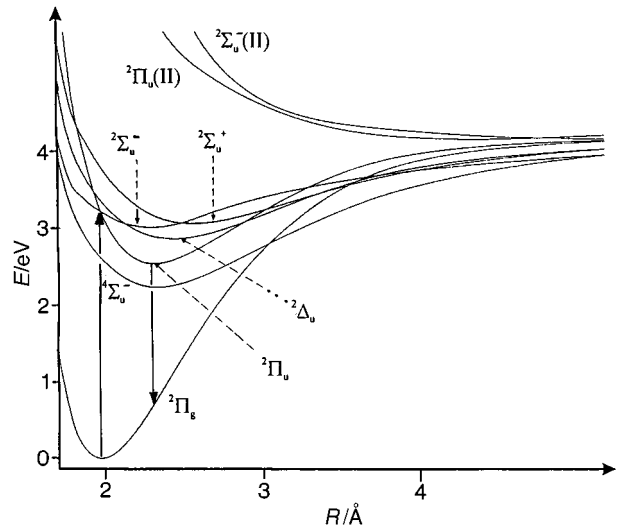

Fig. 8 Potential energy diagram, displaying the low-lying electronic states of S_2^-; the energies are given relative to the ground state minimum and the Franck–Condon transitions $^2\Pi_g \Leftrightarrow {}^2\Pi_u$ in absorption and emission are marked by arrows.

3 Selenium colour centres in zeolitic structures

Basing our method on an old preparation procedure from 1877, which yielded a reddish-brown selenium sodalite,[20] we obtained a brilliant red ultramarine-type solid of pigment quality by optimising the synthesis conditions.[21] The selenium ultramarine is similarly stable to the lapislazuli and does not decompose even on heating to 800 °C under argon, according to colour centres in the zeolitic cages (Fig. 5), which are completely screened from the environment. Though of weaker colour intensity it may eventually substitute red pigments such as Cd(S,Se) (Fig. 9), which has to be withdrawn from the market

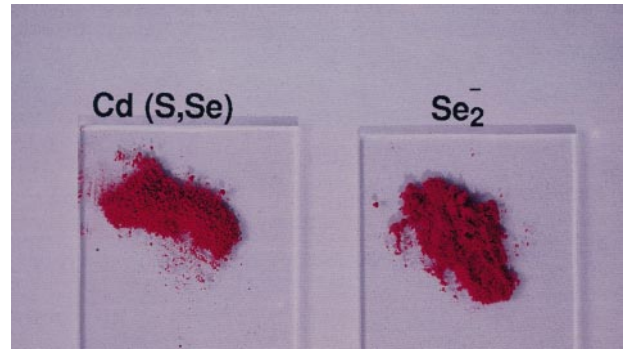

Fig. 9 The red selenium ultramarine in comparison with the industrial pigment $Cd(S_{0.53}Se_{0.47})$ - a mixed crystal between CdS (yellow) and CdSe (black).

for reasons of environment pollution. A typical composition as obtained from electron microscopy and atomic absorption spectroscopy is: $Na_{6.5(2)}[Al_{5.9(1)}Si_{6.1(1)}O_{24}]Se_{2.0(2)}$.

From a resonance Raman study by Clark[22] of a brick-red industrial ultramarine selenium pigment, it was inferred that Se_2^- was the only many-atomic selenium species present. A single progression with 335 cm^{-1} was found, intermediate between the reported vibrational energies of Se_2 (≈ 390 cm^{-1}) and Se_2^{2-} (≅ 250 cm^{-1}). The presence of Se_2^- as the only colour centre is compatible with the above given composition of the red selenium ultramarine within the error range. However,

Se_2^- impurity centres had already been detected in selenium-doped KI single crystals by optical[23a] and Raman spectroscopy[16] earlier. The powder reflection spectra of selenium ultramarines (Fig. 10) show two bands,[21,22] from which only the

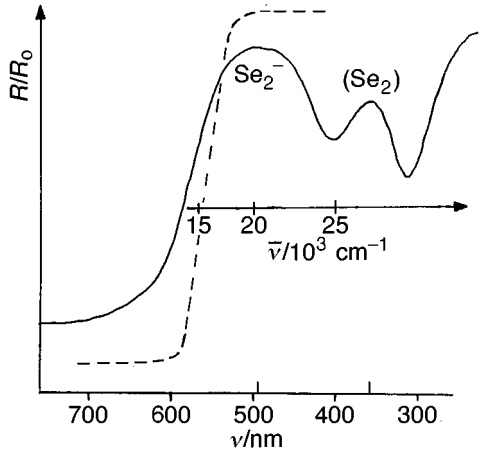

Fig. 10 The powder reflectance spectrum (298 K) of a red selenium ultramarine with the approximate composition $Na_7\square_1[Al_6Si_6O_{24}]Se_2\square_1$ (□: vacancies on positions in the cages); the absorption edge of the red $Cd(S_{0.53}Se_{0.47})$ pigment (Fig. 9) is also indicated (hatched curve).

broad and more intense one at lower energy (≅ 20000 cm^{-1}) correlates with Se_2^-, as will be substantiated below.[24] The red colour originates from the spectral transparency in the visible region below about 17500 cm^{-1}. The same two bands have been reported for Se_2^- doped KI as well.[23b] In Fig. 10 the steep absorption edge of the Cd(S,Se) pigment of Fig. 9 is indicated, whose colour follows from the specific band structure of the mixed crystal. Accordingly a brighter hue results than in cases where the colour is caused by broad bands with less selective absorption properties, due to centres such as S_2^-, S_3^- or Se_2^-.

Quantum chemical calculations similar to those for S_2^-, but approximately including scalar and spin-orbit relativistic effects, were performed for the diselenium radicals as well.[25] The obtained vertical transition energies and relative dipole-transition moments are summarized in Table 1. Nearly the same sequence of states results for Se_2^- as compared to S_2^-, but with transition energies distinctly shifted to lower values by about 20%. The respective potential curves are similar to those of Fig. 8. Without doubt the broad band in the spectrum of ultramarine-red (Fig. 10) corresponds to the $^2\Pi_g \rightarrow {}^2\Pi_u$ transition with presumably intensity contributions from $^2\Pi_g \rightarrow {}^2\Sigma_u^-$, $^2\Delta_u$—in complete analogy to S_2^-. The assignment is confirmed by a single crystal optical study of selenium-doped cancrinite,[26] where this band shows the polarisation behaviour expected for the $^2\Pi_g \rightarrow {}^2\Pi_u$ transition in question (Table 1). The agreement between experiment (≅ 20000 cm^{-1}) and theory is still satisfactory, considering the computational difficulties connected with the electron-rich diselenium system[25] and disregarding the influence of the sodalite matrix. The proposed assignment of the band at 27500 cm^{-1} (Fig. 10) to the $^2\Pi_g \rightarrow {}^2\Sigma_u^+$ transition[23b] has to be rejected, however. On the one hand the disagreement between the experimental data and the calculated intensity and energy values (Table 1) is too large, and on the other hand the emission spectrum of selenium doped sodalite gives evidence that the band originates from the Se_2 diradical (see below). The low-temperature luminescence spectrum in Fig. 11 shows a band at 14000 cm^{-1} with a very well resolved fine-structure, which corresponds to the progression of a vibrational mode with the same energy (335 cm^{-1}) as that observed in the Raman spectrum. It is also in fair agreement with the calculated value for Se_2^- (310 cm^{-1}).[25] The assignment to the $^2\Pi_u \rightarrow {}^2\Pi_g$ transition is hence ensured, the Stokes' shift being about 6500 cm^{-1}, as expected smaller than in the sulfur case.

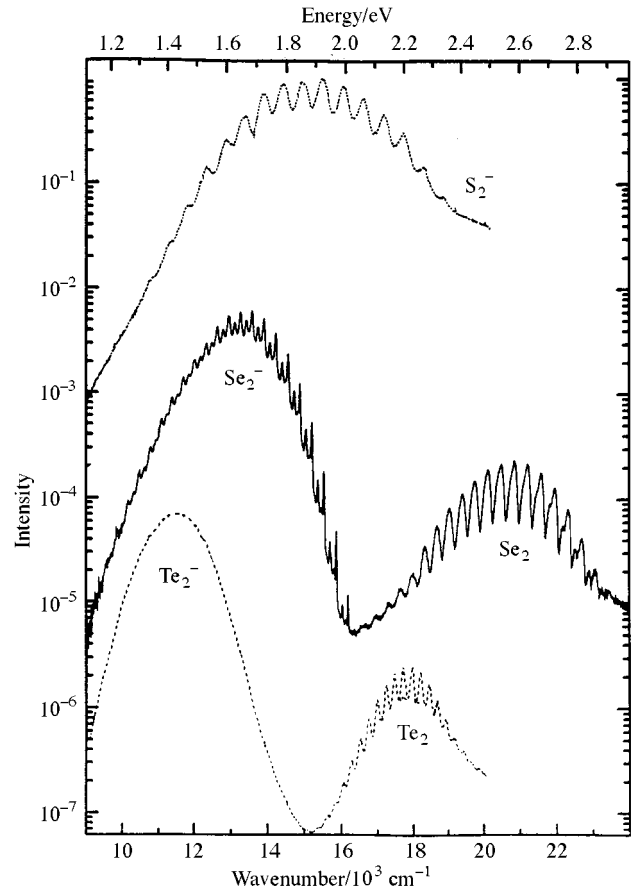

Fig. 11 Luminescence spectra of dichalcogen-doped ultramarine-type solids (< 10 K; laser excitation energy in the sulfur and selenium case: 27500 cm^{-1}, for the green tellurium-doped sodalite: 22000 cm^{-1}); the logarithmic intensity scale enhances the weak emissions ascribed to Se_2 and Te_2.

At higher laser excitation energies (27500 cm^{-1}) a second weak luminescence band at 21000 cm^{-1} shows up (Fig. 11). The progression is with $\bar{\nu}$ = 384 cm^{-1} considerably larger than that in the lower-energy transition and in excellent agreement with the calculated stretching frequency of the neutral Se_2 molecule in the $^3\Sigma_g^-$ ground state (386 cm^{-1}).[25] However, because it is not observed in the Raman and emission spectra at lower laser excitation energies of 20000 cm^{-1}, Se_2 seems to be present only as an intermediate species in the sodalite cages. The low-lying excited triplet states of the Se_2 molecule—only symmetry allowed transitions are considered—are $^3\Sigma_u^-$ and $^3\Pi_u$ (see the potential energy diagram in Fig. 12).[25] From these $^3\Sigma_g^- \rightarrow {}^3\Sigma_u^-$ possesses the much higher transition moment and is calculated to appear at ≈ 27000 cm^{-1}.[25] We may hence readily assign the band at 27500 cm^{-1} in the spectrum of the red selenium ultramarine (Fig. 10) to this transition. In agreement with this assignment it appears in the optical spectrum of selenium-doped cancrinite single crystals,[26] if the incident light is polarised parallel to the *c*-axis.

The proposed mechanism[24] for the generation of intermediate Se_2 species implies (see Fig. 13): (a) the excitation of Se_2^- from the ground state into higher vibrational levels of $^2\Pi_u$, (b) photodetachment and relaxation into the ground state of the neutral Se_2 molecule—note the crossing of the $^2\Pi_u$ (≅ $\pi_u^3\pi_g^4$) and $^3\Sigma_g^-(\pi_u^4\pi_g^2)$ states in Fig. 13—the electron being transferred onto the sodalite frame (see below), (c) excitation of Se_2 into $^3\Sigma_u^-$ by a second UV photon of the same energy (≈ 3 eV) as the one involved in (a), (d) eventually followed by the $^3\Sigma_u^- \rightarrow {}^3\Sigma_g^-$ emission in the luminescence experiment.

It is, at first, surprising that ionisation into the lattice is supposed to occur in the case of selenium, but is not observed for S_2^-—though the adiabatic electron affinity (minimum-to-

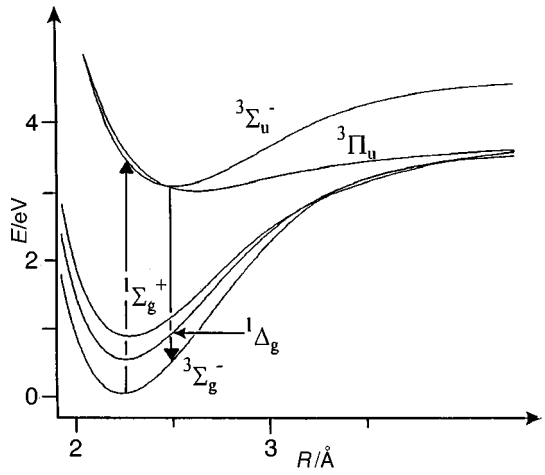

Fig. 12 Potential energy diagram, showing low-lying electronic states of Se_2. The lowest three states mainly originate from $\pi_u^4\pi_g^2$, while $\pi_u^4\pi_g^1\sigma_u^1$ and $\pi_u^3\pi_g^3$ give rise to $^3\Pi_u$ and $^3\Sigma_u^-$ (besides others), respectively (see Fig. 7); the arrows mark the vertical $^3\Sigma_g^- \Leftrightarrow {}^3\Sigma_u^-$ transitions in absorption and emission.

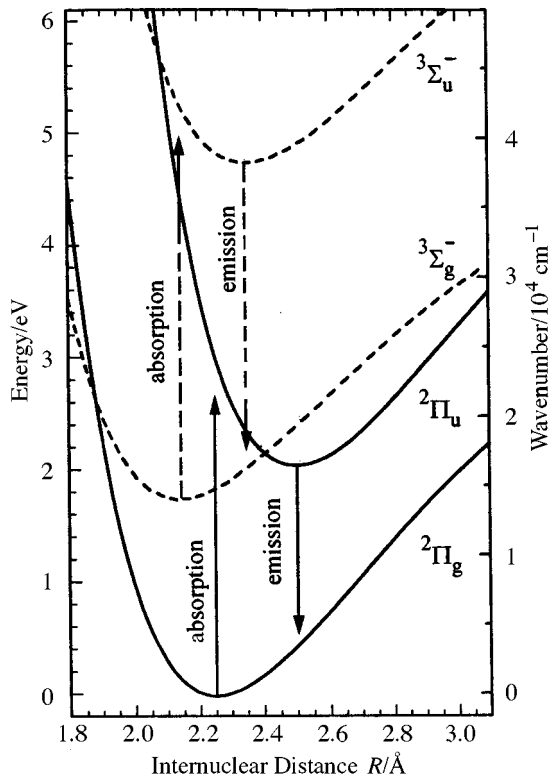

Fig. 13 Potential energy diagram, visualising the generation process of the intermediate Se_2 centre in selenium-doped sodalite, solid and dotted curves refer to Se_2^- and Se_2, respectively (see text).

minimum distance of the respective potential curves) of S_2 (1.67 eV)[18] is smaller than that of Se_2 (1.95 eV).[25] We will consider this interesting matter explicitly in the following.

Fig. 14a displays in the same diagram the $^2\Pi_g \Leftrightarrow {}^2\Pi_u$ and $^3\Sigma_g^- \Leftrightarrow {}^3\Sigma_u^-$ transitions of Se_2^- and Se_2, respectively, in the sodalite matrix in luminescence and absorption. Fig. 14b visualizes the spectral features in the energy region between the two bands originating from the Se_2^- colour centre in high resolution.[24] Two main progressions A and B with identical frequency are clearly visible—the fundamental vibrational energies being 335 cm^{-1} in the $^2\Pi_g$ ground state (as mentioned before) and 225 cm^{-1} in the $^2\Pi_u$ excited state (calculated value:[25] 200 cm^{-1}). The origins (0–0' transitions) of A and B are distinctly different with 16546 cm^{-1} and 16718 cm^{-1}, respectively—but as expected approximately intermediate be-

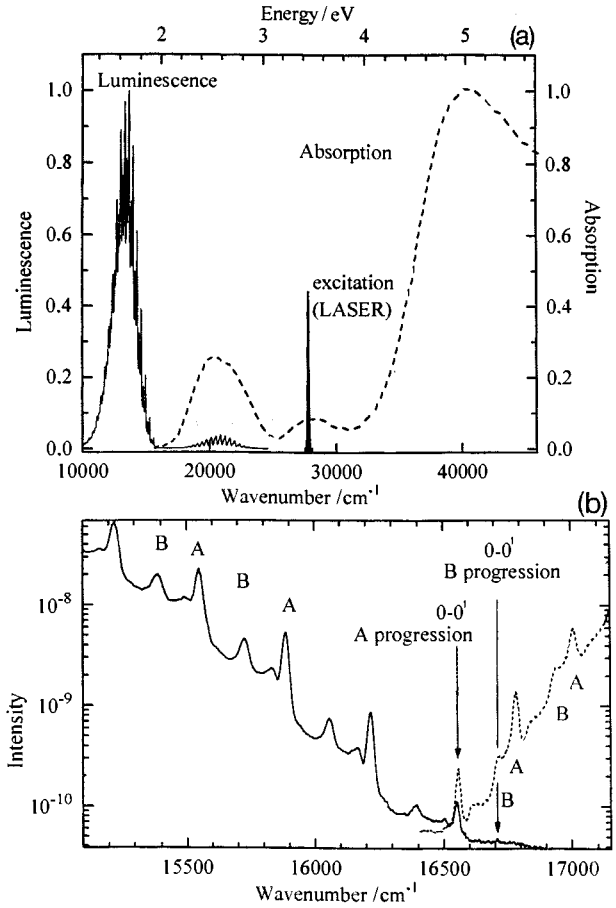

Fig. 14 The $^2\Pi_g \Leftrightarrow {}^2\Pi_u$ transition of Se_2^- and the $^3\Sigma_g^- \Leftrightarrow {}^3\Sigma_u^-$ transition of the intermediate Se_2 centre—red ultramarine-type sodalite—in absorption (hatched spectrum) and luminescence (intensity in arbitrary units); the higher-energy emission band is not seen at lower laser excitation energies (a). The high-resolution photoluminescence (PL) and the photoluminescence-excitation (PLE) spectrum (< 10 K; laser energy: 19500 cm^{-1}) of a selenium-doped sodalite single crystal (solid and dotted lines, respectively) in the region of spectral overlap for the Se_2^- centre (the PLE is equivalent to the absorption spectrum); the 0–0' transitions (0, 0' refer to the lowest vibronic states of $^2\Pi_g$ and $^2\Pi_u$, respectively) of the two progressions A and B (see text) are marked (b).

tween the corresponding absorption and emission band maxima in Fig. 14a. It should be noted here, that for Se_2^- doped KI only one progression is observed in the low-temperature PL and PLE spectra, the 0–0' transition being of the considerably smaller energy 16040 cm^{-1}. We explain these results as follows:[24,25] (a) the comparatively high transition energies indicate the presence of steric constraints in the sodalite matrix due to a mismatch between the Se_2^- volume and the cage size. This is also apparent in the strongly reduced occupancy of the cages by Se_2^- in the red selenium ultramarines. This argument was also used with respect to, in particular, the S_3^- colour centres in the blue sulfur ultramarines. (b) The origin of the two progressions is proposed to be caused by two different polyhedron species $[Se_2^- Na_3]^{2+}$ and $[Se_2^- Na_4]^{3+}$ in the sodalite cages, which may be verified by considering the approximate composition of the selenium ultramarine in Fig. 10 with vacancies not only on the Cl^-, but on the Na^+ positions as well. They are assigned to progressions A and B, respectively—having in mind that the former colour centre is expected to undergo less severe steric strains due to the incomplete tetrahedral Na^+ coordination. It is present in higher concentrations (see the A/B intensity ratio in Fig. 14b). (c) The mentioned steric constraints favour the ionisation of Se_2^- into the lattice, leaving a distinctly less voluminous neutral Se_2 diradical. The detached electron is stabilised by delocalisation particularly into neighbouring non-occupied Na_4^+ tetrahedra of the sodalite frame (eqn. (2)). The

$$[Se_2^- Na_3]^{2+} + [Na_4]^{4+} \longrightarrow [Se^0{}_2 Na_3]^{3+} + [e^- Na_4]^{3+} \quad (2)$$

smaller S_2^- radical is not subject to steric constraints of this kind and remains unchanged in the sodalite matrix—in contrast to S_3^-, where steric strains enforce strongly reduced occupancies of the cages as well (see the composition of the violet–blue ultramarine of Fig. 2). (d) The assignment of A and B to split states of $^2\Pi_g$, $^2\Pi_u$ due to crystal field effects from the sodalite host solid can be refuted.[24]

Interestingly enough selenium species can be incorporated into the cancrinite lattice (Fig. 6) as well, yielding red–brown single crystals.[26] The Raman spectrum is indicative of a species with the vibrational mode $\bar{\nu}$ = 244 cm^{-1} and of a minor fraction of Se_2^- ($\bar{\nu}$ = 330 cm^{-1}). The single crystal optical spectrum shows an intensity-dominating band at 24000 cm^{-1}, which is apparently unpolarised, besides strongly polarized absorption features characteristic of Se_2^- radical anions, aligned parallel to the channel axis. The observed low-energy vibration suggests Se_2^{2-} to be the main colour centre present, though the band at 24000 cm^{-1} cannot be definitely assigned—the process $Se_2^{2-} \rightarrow Se_2^-$ is exothermic.[25]

According to quantum chemical calculations Se_3^- should exist as a stable species in the open form of C_{2v} symmetry, as S_3^-.[25] The vertical excitation energy of the most intense symmetry-allowed $^2B_1 \rightarrow {}^2A_2$ transition is expected at 12500 cm^{-1}. Very probably for steric reasons this species is observed neither in the sodalite (see Fig. 10) nor in the cancrinite host matrix.

4 Tellurium colour centres in zeolitic cage structures

It is also possible to incorporate ditellurium species into the cages of sodalite-type solids,[27] though severe steric strain effects are expected due to the mismatch between the cage size and the dimensions of the colour centres. We have noticed this before when discussing the spectroscopic features of Se_2^- in the same matrix. Most certainly, steric constraints are also the reason why only tellurium ultramarines can be synthesized, in which at least half of the cages are still centered by Cl^- anions—in contrast to the situation in the sulfur and selenium case. Nevertheless up to 25% of the cages can be occupied by ditellurium species. It might be interesting to speculate on the coordination of the X_2 and X_2^- radicals in the sodalite host. The Cl^-–Na^+ spacings within the $[ClNa_4]^{3+}$ tetrahedra of S_4 symmetry are 2.73 Å, while the next-nearest distance from the cage centre to Na^+ cations in neighbouring cages is 4.96 Å. Having in mind that the incorporation of the heavier dichalcogen species into the sodalite matrix is connected with a Na^+-deficiency, we may postulate the presence preferentially of $[X_2^{(-)}Na_3]^{3+(2+)}$ polyhedra as the colour centres (see Section 3). The most reasonable geometry is trigonal planar, with the $X_2^{(-)}$ entities oriented perpendicular to the Na_3^{3+} plane (Fig. 15)—equally for electrostatic and steric reasons. Adopting ionic radii of 1.75 and 0.98 Å for Cl^- and Na^+, respectively, the available space within the Na_3^{3+} plane, where also the bond overlap region of X_2 and X_2^- is located, is ≅ 0.60 Å. Steric constraints should be particularly distinct for the large Te_2^- centre, as can be deduced from Table 2, where calculated bond lengths for the X_2 and X_2^- radicals in question are given. The proposed coordination geometry also readily explains the relative instability of X_2^- with respect to X_2, which can be largely traced back to the repulsive electrostatic interaction between X_2^- and the negatively charged cage frame.

Depending on the detail of the preparation procedure for tellurium ultramarines, blue to greenish products are obtained. Typical powder reflection spectra are displayed in Fig. 16. Both solids show the same strong band at 16500 cm^{-1}, while the absorption features between 21000 and 25000 cm^{-1} are more intense in the former case, but are structured identically, as the

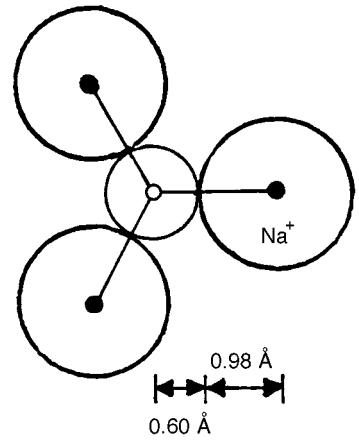

Fig. 15 Available space for dichalcogen radicals in the sodalite cages, if cation-deficient $[X_2^{(-)}\ Na_3]^{3+(2+)}$ polyhedra are assumed (orientation of $X_2^{(-)}$ perpendicular to Na_3-plane, see text).

insert nicely shows. The blue compound exhibits a Raman spectrum with a progression up to the 8th order of the fundamental vibrational energy of 230 cm^{-1} (Fig. 17a). At a slightly higher laser energy within the reach of the broad absorption band around 23(±2) × 10^3 cm^{-1} a second progression comes up, based on a fundamental vibration of 247 cm^{-1} (Fig. 17b). The luminescence spectrum displays two bands, similar to that of the selenium ultramarine, but shifted to lower energies (Fig. 11). We may readily assign the absorption band at 16500 cm^{-1} and the lower-energy emission at 11500 cm^{-1} to the $^2\Pi_g \Leftrightarrow {}^2\Pi_u$ transition of a Te_2^- colour centre. Surprisingly at first sight, the luminescence band lacks vibrational fine structure. Obviously, it is smeared out due to severe destabilizing interactions of the voluminous Te_2^- radical with the sodalite lattice framework. Quantum chemical calculations, including in an approximate manner scalar relativistic and spin-orbit coupling effects,[28] predict the vertical transition to appear at 14500 cm^{-1}, deviating from the experimental value more strongly than in the selenium case. One should remember that Se_2^- is already the subject of steric constraints, which have distinctly enhanced the $^2\Pi_g \Leftrightarrow {}^2\Pi_u$ transition energy (the difference between the 0–0' transitions of Se_2^- in the sodalite matrix and doped into KBr was 500–700 cm^{-1}, see Section 3). Thus the mismatch between the experimental and theoretical transition energy, calculated without taking matrix influences into account, is indeed expected to be more distinct for Te_2^- (see Table 2). The same argument holds for the calculated energy of the Te_2^- stretching mode (205 cm^{-1}),[28] which is appreciably smaller than the observed value (230 cm^{-1}) as well.

The higher energy bands in the absorption (≈ 23000 cm^{-1}) and luminescence spectra should—again analogously to the selenium ultramarine—originate from the neutral Te_2 diradical. The vertical $^3\Sigma_g^- \rightarrow {}^3\Sigma_u^-$ transition is calculated at ≅ 24000 cm^{-1} (see Fig. 13),[28] close to the experimental value. The Te_2 stretching frequency as deduced from the Raman spectrum (Fig. 17b) and from the vibrational progression of the higher-energy luminescence band at 18000 cm^{-1} (Fig. 11) is 247(±3) cm^{-1}, in very good agreement with the calculated energy of 252 cm^{-1}.

While the experimental evidence for the blue tellurium ultramarine indicates the presence of Te_2^- colour centres and

Table 2 Calculated[18,25,28] interatomic distances in free X_2 and X_2^- radicals (Å)

S_2	1.91
S_2^-	2.02
Se_2	2.18
Se_2^-	2.31
Te_2	2.57
Te_2^-	2.70

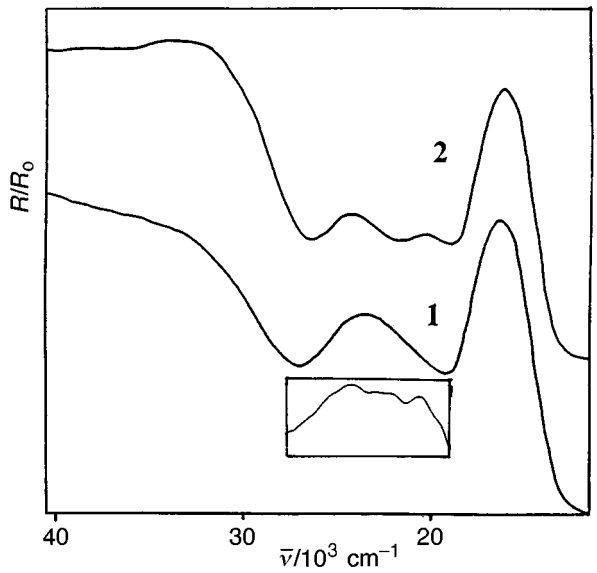

Fig. 16 Powder reflectance spectra (298 K) of a greenish (1) and a blue (2) tellurium ultramarine (arbitrary reflectance intensity scale); the insert shows the 5 K-spectrum of (1) between 19 and 28 × 10^3 cm^{-1}.

intermediate Te_2 centres as in the selenium case, the situation is different for the green solid. Here, the Raman spectrum shows already at lower laser energies two progressions,[27] similar to Fig. 17b, and we may conclude that Te_2 is incorporated into the sodalite cages as a stable centre in this compound. This result is in agreement with the higher intensity of the absorption band at ≈ 23000 cm^{-1} for the green compared to the blue ultramarine. The broad and structured appearance of the latter transition (Fig. 16) might be due to the calculated near-coincidence of the intense $^3\Sigma_g^- \rightarrow {}^3\Sigma_u^-$ with the weak $^3\Sigma_g^- \rightarrow {}^3\Pi_u$ transition (see Fig. 12) and their mixing *via* the strong spin-orbit coupling in the electron-rich tellurium system. Further theoretical and experimental studies are needed.

5 Summary and conclusions

It is not only possible to substitute S_2^- and S_3^- radical anions into the cages of the sodalite and related structures as has long been known, but also various colour centres of the heavier chalcogens can be used, such as Se_2, Se_2^-, Se_2^{2-}, Te_2 and Te_2^-. Zeolitic solids containing cages, which are well-screened from atmospheric influences, are ideal matrices for stabilising and isolating such paramagnetic centres, which would decompose rapidly otherwise. Suitable and effective probe methods are particularly spectroscopic techniques, including Raman, optical and EPR spectroscopy. Further attractive aspects are the colour and luminescence properties of compounds of this type, which might be used as industrial pigments and solid state lasers, respectively.

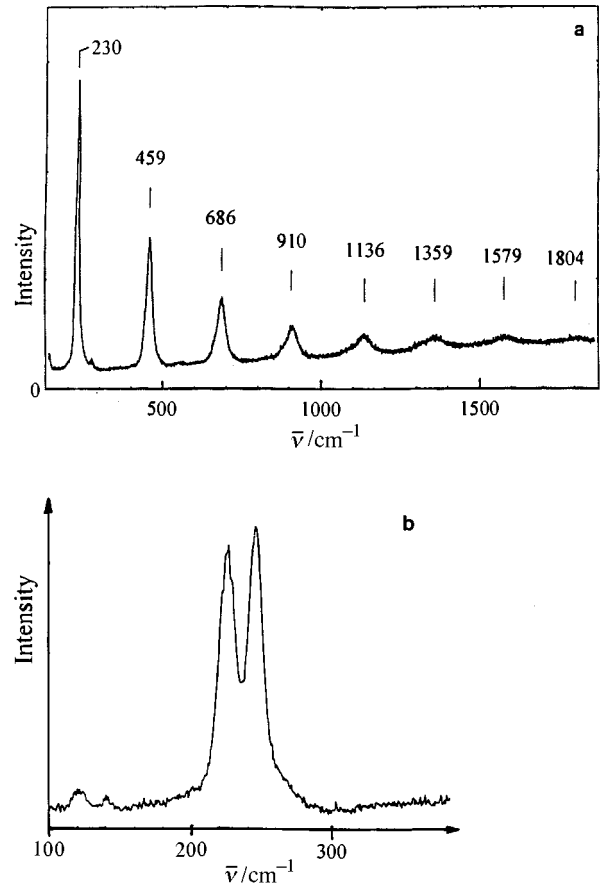

Fig. 17 Raman spectra of the blue tellurium ultramarine, excited with the (a) 19500 cm^{-1} (1 mW power level) and with the (b) 20500 cm^{-1} laser line (2 mW power level).

Table 3 gives an overview of some important energetic properties of dichalcogen centres in the cages of zeolitic hosts. The agreement between observed and calculated energies is mostly satisfactory, with the exception of Se_2^- and Te_2^-. Here, the values from theory are too low, which may be partially caused by electrostatic and steric constraints of these centres in the sodalite cages—as has been explicitly discussed. The Stokes' shift decreases from S_2^- (≈ 10000 cm^{-1}) *via* Se_2, Se_2^- (6000 cm^{-1}) to Te_2, Te_2^- (5000 cm^{-1}); this is expected because the displacements of the potential energy curves in the ground and the excited states along the internuclear distance coordinate (Figs. 8,12) decrease toward the heavier chalcogens. After all, one may state that the electronic properties of dichalcogen radicals X_2, X_2^- in zeolitic cage structures are, sometimes even in the finer details, quite well understood. The calculated potential energy curves and transition energies[18,25,28] indicate,

Table 3 Transition energies for absorption and emission, and vibrational energies of dichalcogen species X_2, X_2^-, X_2^{2-} (X = S, Se, Te) mostly in zeolitic host solids; experimental[14, 21, 24, 27] and calculated[18, 25, 28] energies are given (ranges of experimental observation in parentheses)

		Transition energy for $^3\Sigma_g^- \Leftrightarrow {}^3\Sigma_u^-/10^3$ cm^{-1}		Vibrational energy $\bar{\nu}(^3\Sigma_g^-)/cm^{-1}$			Transition energy for $^2\Pi_g \Leftrightarrow {}^2\Pi_u/10^3$ cm^{-1}		Vibrational energy $\nu(^2\Pi_g)/cm^{-1}$			Vibrational energy $\nu(^1\Sigma_g^+)/cm^{-1}$
		Absorption	Emission				Absorption	Emission				
S_2	exp	—	—	726 (ref. 29)	S_2^-	exp.	26	~16	600	S_2^{2-}	exp.	450 (ref. 30)
	calc.	—	—	734		calc.	25.2	—	582		calc.	—
Se_2	exp.	27.5	21	384	Se_2^-	exp.	20[a]	14[a]	335	Se_2^{2-}	exp.	248 (±4)
	calc.	27.0	—	386		calc.	18.6	—	310		calc.	—
Te_2	exp.	~23	18	247 (±3)	Te_2^-	exp.	16.5	11.5	228 (±2)	Te_2^{2-}	exp.	188 (±2)
	calc.	24	—	252		calc.	14.5	—	205		calc.	—

[a] 0–0′ transitions at 16 718, 16 546 and 16 040 cm^{-1} for the B, A centres in sodalite and for Se_2^--doped KI, respectively.

for example, that the one-electron energy differences between σ_u and π_g and π_g and π_u in the MO scheme of Fig. 7 are about equal.

Our attempts so far to incorporate di- or trioxygen entities into the sodalite matrix yielded only products with a weakly reddish colour, which might originate from traces of O_3^- centres as the spectroscopic data suggest.[12] This is surprising, because O_2^- and O_3^- are rather stable radical anions, compared to corresponding species of the heavier chalcogens. Thus for example, the bright orange–red to red alkaline and tetraalkylammonium ozonide salts are well-known and have recently been structurally and spectroscopically characterised.[31] The colour-determining broad band around $20(\pm1) \times 10^3$ cm^{-1} (in solution at $\cong$ 21500 cm^{-1} and calculated[32] at 22300 cm^{-1}) is found at a higher energy, by $\approx$ 4000 cm^{-1}, than the analogously assigned transition of S_3^- in the blue sulfur ultramarines (see Section 2).

We also did not succeed in preparing ultramarines with mixed chalcogen radicals, such as $(SSe)^-$ for example. As

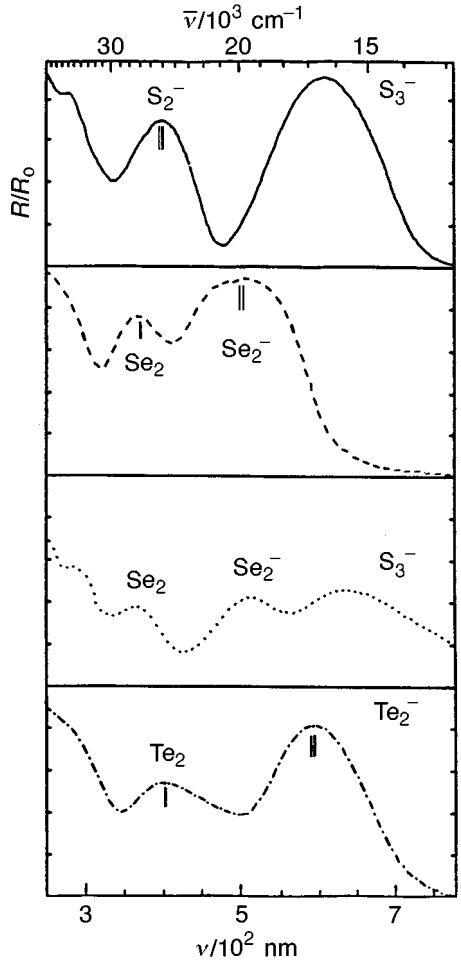

Fig. 18 Powder reflectance spectra of various ultramarine-type solids with chalcogen radicals (colour centres indicated); the colours are, from above: green, red, brown (no mixed S/Se centres are observed, see text) and green.

Fig. 18 shows, the resulting colour centres were separate S_3^- and Se_2^- (Se_2) entities. This result contrasts with that reported for sulfur- and selenium-doped KI, where the Raman spectra indicate the presence of SeS^- beside S_2^- and Se_2^-.[16] The vibrational energy of the former radical anion (465 cm^{-1}) is intermediate between those of the two latter species (Table 3). Fig. 18 also illustrates that the optical spectra are rough but efficient fingerprints for the identification of chalcogen-type species, which can be quickly obtained. A wide range of colours is generated by the variation of X (S, Se, Te), the composition (S_2^-, S_3^-) and the charge (Te_2^-, Te_2) of the radical molecule or anion.

6 Acknowledgements

It is a pleasure for the authors to thank Professor W. Koch and Dr Heinemann (TU Berlin) for their expert support from the quantum mechanical side, which has contributed essentially to the understanding of the spectroscopic properties of the title compounds. We further gratefully acknowledge the specialist help of Dr K. Witke (Bundesanstalt für Materialforschung und -prüfung, Berlin) concerning Raman spectroscopy and finally thank Professor W. Koch again for critically reading the manuscript.

7 References

1 W. Noll, *Chem. Unserer Zeit*, 1980, **14**, 37.
2 F. Seel, G. Schäfer, H. J. Güttler and G. Simon, *Chem., Unserer Zeit*, 1974, **8**, 65; F. Seel, *Stud. Inorg. Chem*., 1984, **5**, 67.
3 J. B. Guimet, *Bull. l'enconragem. l'industrie nation*., 1828 (see also ref. 20).
4 J. Riederer, *Naturwissenschaften*, 1982, **69**, 82.
5 G. Bayer and H.-G. Wiedemann, *Sandoz Bulletin*, 1976, **40**, 20.
6 (*a*) M. José-Yacaman, L. Rendón, J. Arenas and M. C. Serra Puce, *Science*, 1996, **273**, 223; (*b*) D. Reinen, P. Demel and P. Köhe, *Z. Anorg. Allg. Chem.*, in the press.
7 A. Ludi, *Chem. Unserer Zeit*, 1988, **22**, 123.
8 D. Reinen, T. C. Brunold, H. U. Güdel and N. D. Yordanov, *Z. Anorg. Allg. Chem*., 1998, **624**, 438.
9 P. Kienbaum, *Chem. Unserer Zeit*, 1986, **20**, 182.
10 S. Di Gregorio, M. Greenblatt, J. Pifer and M. D. Sturge, *J. Chem. Phys*., 1982, **76**, 2931.
11 (*a*) P. Chandley, R. J. H. Clark, R. J. Angel and G. D. Price, *J. Chem. Soc., Dalton Trans*., 1992, 1579; (*b*) A. Siggel and M. Jansen, *Z. Anorg. Allg. Chem*., 1990, **583**, 67.
12 G.-G. Lindner, *Thesis*, University of Marburg, Verlag Shaker 1994.
13 A. S. Sofianides and G. E. Harlow, Eds., *Gems and Crystals from the American Museum of Natural History, New York*, Simon and Schuster Inc., New York 1990 (the authors gratefully acknowledge permission to use the figure).
14 R. J. H. Clark and D. G. Cobbold, *Inorg. Chem*., 1978, **17**, 3169, and references therein.
15 L. E. Vanotti, *Phys. Rev*., 1967, **161**, 282; J. Schneider, B. Dischler and A. Räuber, *Phys. Status Solidi*, 1966, **13**, 141.
16 W. Holzer, W. F. Murphy and H. J. Bernstein, *J. Mol. Spectrosc*., 1969, **32**, 13.
17 G.-G. Lindner, W. Massa and D. Reinen, *J. Solid State Chem*., 1995, **117**, 386.
18 C. Heinemann, W. Koch, G.-G. Lindner and D. Reinen, *Phys. Rev. A*, 1995, **52**, 1024.
19 W. Koch, J. Natterer and C. Heinemann, *J. Chem. Phys*., 1995, **102**, 6159.
20 J.-F. Plique, *Bl. Soc. Chim. Paris N.S.*, 1877, **28**, 522; E. Guimet, *Bl. Soc. Chim. Paris N.S.*, 1878, **29**, 99 and 104.
21 G.-G. Lindner and D. Reinen, *Z. Anorg. Allg. Chem*., 1994, **620**, 1321.
22 R. J. H. Clark, M. T. Dines and M. Kurmoo, *Inorg. Chem*., 1983, **22**, 2766.
23 (*a*) M. Ikezawa and J. Rolfe, *J. Chem. Phys*., 1972, **58**, 2024; G. J. Vella and J. Rolfe, *J. Chem. Phys*., 1974, **61**, 41; (*b*) H. Murata, T. Kishigami and R. Kato, *J. Phys. Soc. Jpn*., 1990, **59**, 506.
24 H. Schlaich, G.-G. Lindner, J. Feldmann, E. O. Göbel and D. Reinen, *J. Inorg. Chem*., in the press.
25 C. Heinemann, W. Koch, G.-G. Lindner, D. Reinen and P.-O. Widmark, *Phys. Rev. A*, 1996, **54**, 1979, and references therein.
26 G.-G. Lindner, K. Hoffmann, K. Witke, D. Reinen, C. Heinemann and W. Koch, *J. Solid State Chem*., 1996, **126**, 50.
27 G.-G. Lindner, K. Witke, H. Schlaich and D. Reinen, *Inorg. Chim. Acta*, 1996, **252**, 39.
28 C. Heinemann, W. Koch and P.-O. Widmark, *Mol. Phys*., 1997, **92**, 463.
29 G. Herzberg, *Molec. Spectra and Molec. Structure, Vol. I, Spectra of Diatomic Molecules*, 1989, Krieger, Malabar, FL.

30 P. Böttcher, J. Getzschmann and R. Keller, *Z. Anorg. Allg. Chem.*, 1993, **619**, 476.
31 W. Assenmacher and M. Jansen, *Z. Anorg. Allg. Chem.*, 1998, **624**, 661.
32 W. Koch, G. Frenking, G. Steffen, D. Reinen, M. Jansen and W. Assenmacher, *J. Chem. Phys.*, 1993, **99**, 1271.

Review 7/04920J